AD-A166 484 FERROELECTRIC TUNGSTEN BRONZE CRYSTALS FOR FAR INFRARED ELECTRO-OPTIC DEV (U) ROCKWELL INTERNATIONAL ANAHEIM CA SCIENCE CENTER R R NEURGAONKAR NOV 85 SC5356.56FR 1/1

UNCLASSIFIED DAAK70-83-C-0016 F/G 20/2 NL

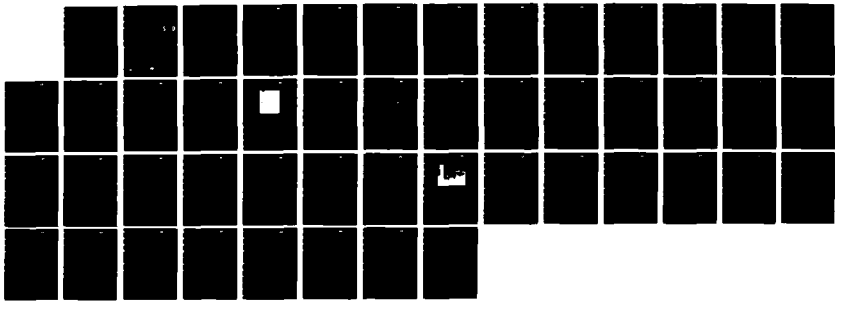

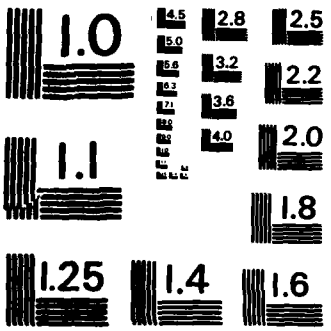

FERROELECTRIC TUNGSTEN BRONZE CRYSTALS FOR FAR INFRARED ELECTRO-OPTIC DEVICE APPLICATIONS

(2) 9

FINAL TECHNICAL REPORT FOR THE PERIOD
January 12, 1983 through September 30, 1985

NOVEMBER 1985

NVEL ORDER:	
EFFECTIVE DATE OF CONTRACT:	**01/12/83**
CONTRACT EXPIRATION DATE:	**09/30/85**
AMOUNT OF CONTRACT DOLLARS:	**$143,906**
CONTRACT NUMBER:	**DAAK70-83-C-0016**
PROJECT NUMBER:	**2131**
PRINCIPAL INVESTIGATOR:	**DR. R.R. NEURGAONKAR (805) 373-4109**

Prepared for

U.S. Army Belvoir Research and Development Center
Fort Belvoir, VA 22060

Sponsored by

Night Vision Electro-Optic Laboratory (NVEL)
NVEL Order No.

Rockwell International
Science Center

UNCLASSIFIED
SECURITY CLASSIFICATION OF THIS PAGE

ADA 166 484

REPORT DOCUMENTATION PAGE

1a. REPORT SECURITY CLASSIFICATION Unclassified	1b. RESTRICTIVE MARKINGS
2a. SECURITY CLASSIFICATION AUTHORITY	3. DISTRIBUTION/AVAILABILITY OF REPORT Approved for public release; distribution unlimited.
2b. DECLASSIFICATION/DOWNGRADING SCHEDULE	
4. PERFORMING ORGANIZATION REPORT NUMBER(S) SC5356.56FR	5. MONITORING ORGANIZATION REPORT NUMBER(S)
6a. NAME OF PERFORMING ORGANIZATION Rockwell International Science Center 6b. OFFICE SYMBOL (If applicable)	7a. NAME OF MONITORING ORGANIZATION Night Vision Electro-Optic Laboratory (NVEL)
6c. ADDRESS (City, State and ZIP Code) 1049 Camino Dos Rios Thousand Oaks, CA 91360	7b. ADDRESS (City, State and ZIP Code)
8a. NAME OF FUNDING/SPONSORING ORGANIZATION U.S. Army Belvoir Research and Development Center 8b. OFFICE SYMBOL (If applicable)	9. PROCUREMENT INSTRUMENT IDENTIFICATION NUMBER Contract No. DAAK70-83-C-0016
8c. ADDRESS (City, State and ZIP Code) Fort Belvoir VA 22060	10. SOURCE OF FUNDING NOS PROGRAM ELEMENT NO. / PROJECT NO. 2131 / TASK NO. / WORK UNIT NO.
11. TITLE (Include Security Classification) FERROELECTRIC TUNGSTEN BRONZE CRYSTALS FOR FAR INFRARED ELECTRO-OPTIC DEVICE APPLICATIONS (U)	
12. PERSONAL AUTHOR(S) Neurgaonkar, R.R.	
13a. TYPE OF REPORT Final Report 13b. TIME COVERED FROM 01/12/83 TO 09/30/85	14. DATE OF REPORT (Yr., Mo., Day) NOVEMBER 1985 15. PAGE COUNT 39
16. SUPPLEMENTARY NOTATION	
17. COSATI CODES FIELD / GROUP / SUB. GR.	18. SUBJECT TERMS (Continue on reverse if necessary and identify by block number)

19. ABSTRACT (Continue on reverse if necessary and identify by block number)

Several undoped and doped tungsten bronze BSKNN-1 and BSKNN-2 single crystals have been grown by the Czochralski technique. Optical evaluation shows that both the crystals show minimum striations, and are useful for optical studies. Current growth results suggest that the existence of striations depends on the type of dopant and the purity of starting materials. Both BSKNN-1 and BSKNN-2 crystals show excellent ferroelectric and optical properties which are similar to perovskite $BaTiO_3$ rather than to tungsten bronze SBN:60 single crystals. The unit cells for BSKNN-1 and BSKNN-2 are slightly bigger than SBN:60 crystal and for these small changes their entire ferroelectric properties are different. For example, ϵ_{11}, d_{15} and r_{51} are larger for BSKNN crystals while the ϵ_{33}, d_{33} and r_{33} are larger for smaller unit cell SBN:60 single crystals. Further work is in progress to identify the differences in these bronze crystals.

20. DISTRIBUTION/AVAILABILITY OF ABSTRACT UNCLASSIFIED/UNLIMITED ☒ SAME AS RPT. ☐ DTIC USERS ☐	21. ABSTRACT SECURITY CLASSIFICATION Unclassified
22a. NAME OF RESPONSIBLE INDIVIDUAL	22b. TELEPHONE NUMBER (Include Area Code) / 22c. OFFICE SYMBOL

DD FORM 1473, 83 APR EDITION OF 1 JAN 73 IS OBSOLETE.

UNCLASSIFIED
SECURITY CLASSIFICATION OF THIS PAGE

TABLE OF CONTENTS

LIST OF FIGURES

LIST OF TABLES

1.0 OBJECTIVE

The primary objective of this research program is to develop for electro-optic and nonlinear optical applications high quality, striation-free crystals of a number of interesting tungsten bronze compositions such as $Ba_{(2-x)}Sr_xK_{1-y}Na_yNb_5O_{15}$ (BSKNN), $Ba_6Ti_2Nb_8O_{30}$ (BTN), and a few compositions which are close to a morphotropic phase boundary, using the Czochralski and edge defined crystal growth techniques. The large transverse and longitudinal electro-optic response obtainable near morphotropic phase boundaries are ~~to be~~ studied in particular detail for optical device applications. A second objective is to improve material photorefractive performance using selected dopants. These tunsten bronze crystals should have a significant impact on the following device areas:

1. Electro-optics: Modulators and Optical Wave guides.
2. Photorefractive: Holographic Storage, Image Processing, Optical Computing

Coupled with this program, a thermodynamic phenomenological model is to be used to systemize the electro-optic and nonlinear optical properties of the bronze crystals and predict compositions which will be optimum for particular device applications.

2.0 SUMMARY AND PROGRESS

Tungsten bronze (T.B.) family crystals have been shown to be useful for a number of device applications, including electro-optics, nonlinear optical, pyroelectric and high frequency dielectrics. The current work focusses on the development of good quality (acceptable for proposed device studies) $Ba_{1.2}Sr_{0.8}K_{0.75}Na_{0.25}Nb_5O_{15}$ (BSKNN-1), $Ba_{0.5}Sr_{1.5}Ka_{0.5}Na_{0.5}Nb_5O_{15}$ (BSKNN-2), and morphotropic phase boundary (MPB) compositions. Considerable progress has been made in several areas, including the growth of BSKNN crystals, films and the characterization of their ferroelectric and optical properties. Based on current work, a number of dopants have also been identified for photorefractive applications. This work also includes the continued effort to research for new T.B. systems and to identify MPB compositions for photorefractive and electro-optic applications.

Several doped and undoped BSKNN-1 and BSKNN-2 single crystals have been grown by the Czochralski technique, and crystals as large as 1 to 1.5 cm in diameter have been successfully developed. The crystal quality and striations seem to depend strongly on the type of dopant incorporated and the quality of the starting materials. Recently, we eliminated several of these problems for both BSKNN-1 and BSKNN-2 compositions and reasonable quality crystals are now being developed. In parallel, several Ce-doped BSKNN-1 crystals have also been grown to study the role of Ce^{3+} on photorefractive sensitivity and speed. The growth of Ce-doped crystals has been successful, and further efforts are underway to now obtain striation-free crystals.

The ferroelectric and piezoelectric properties of these compositions have been measured and compared with other bronze crystals such as SBN:60, SBN:50 and $Sr_2KNb_5O_{15}$. It is interesting to note that these properties, e.g., ε_{33}, d_{33}, ε_{11}, d_{15}, are significantly different from smaller to bigger unit cell bronzes. For example, ε_{11} and d_{15} are significantly larger for BSKNN-1 and BSKNN-2, while ε_{33} and d_{33} are larger for SBN:60, SBN:50 and SKN. Since the piezoelectric strain coefficient d_{15} behaves similarly to the electro-optic

coefficients r_{51} or r_{42}, it is expected that bigger unit cell bronzes, e.g., BSKNN-1 and BSKNN-2, should have electro-optic and photorefractive properties similar to those seen for $BaTiO_3$ and $KNbO_3$ crystals. It is therefore expected that the development of these bronze crystals will open up a variety of new device concepts, and will provide basic understanding of the electro-optic and photorefractive mechanisms which are presently difficult to obtain using $BaTiO_3$ or $KNbO_3$ crystals. The latter perovskite materials are extremely difficult to prepare, and it is anticipated that the development of these new bronze crystals will have a significant scientific impact on future optical device concepts.

Another alternative approach to the development of improved photorefractive materials is the use of morphotropic phase boundary (MPB) composition crystals, i.e., materials having unusually large electro-optic effects. In the present program we have investigated a few MPB systems such as $Pb_2KNb_5O_{15}$-$Sr_2KNb_5O_{15}$, $PbNb_2O_6$-$Sr_2NaNb_5O_{15}$, etc., which appear to be promising for photorefractive applications. The development of these tungsten bronze materials could have an important impact on future device concepts and designs.

In order to establish the liquid phase epitaxial (LPE) technique for these bronze compositions, it is important to identify suitable flux systems. Extensive work has been performed on the flux systems BSKNN-KVO_3, BSKNN-$NaVO_3$, BSKNN-$Ba_2B_8O_{13}$, BSKNN-$LiVO_3$, etc., and it was found that the vanadium-containing fluxes are superior for bronze BSKNN compositions for several reasons. For example, the supercooling range for vanadium-containing solvents is large, on the order of 40°C or more. Furthermore, the vanadium-containing solvents melt at relatively low temperatures; hence there is a potential for growth of defect-free films. The system BSKNN-KVO_3 has been elected for study and the growth of BSKNN films has been shown successful on BSKNN and SBN:50 substrates. The quality of these films appears to be reasonable and further work should improve film quality and ferroelectric properties. Since the supply of BSKNN and SBN:50 bulk crystals is limited

(most of these crystals are being used for a variety of applications), work on improved film quality has not yet progressed. However, the current work is strongly indicative that if it is necessary to use these films for device configurations, one can, in a relatively short time, further develop these films.

3.0 DEVELOPMENT AND CHARACTERIZATION OF OPTICAL QUALITY T.B. BSKNN CRYSTALS

3.1 Ferroelectric Tungsten Bronze Family Crystals

Ferroelectric tungsten bronze oxides have been studied for their electro-optic and pyroelectric properties and have been found to be most useful for these applications. The bronze compositions can be represented by the general formulae $(A_1)_4(A_2)_2C_4B_{10}O_{30}$ and $(A_1)_4(A_2)_2B_{10}O_{30}$, in which A_1, A_2, C and B are 15-, 12-, 9- and 6-fold coordinated sites in the structure. The tetragonal bronze prototypic structure is shown in Fig. 1 in projection on the (001) plane.[1] A wide range of solid solutions can be obtained by the substitution of different A_1, A_2 and B cations,[2] and a number of different types of ferroelectric and ferroelastic phases have been identified (over 100 compounds and numerous solid solutions). The ferroelectric phases can be divided into two groups: those with tetragonal symmetry (4mm) which are ferroelectric:paraelectric; and those with orthorhombic symmetry (mm2) which are both ferroelectric and ferroelastic. Because of such diversity, there are a number of orthorhombic ($Pb_2KNb_5O_{15}$, $Sr_2NaNb_5O_{15}$, etc.) and tetragonal (SBN:60, SBN:75, SBN:50, BSKNN, KLN, etc.) tungsten bronze crystals available for optical, nonlinear optical and pyroelectrical applications. At Rockwell, attempts are being made to understand the problems associated with the growth of these bronzes. In the present program, the pseudo-binary systems $Sr_{0.75}Ba_{0.25}Nb_2O_6$-$K_{0.5}Na_{0.5}NbO_3$ and $Sr_{0.4}Ba_{0.6}Nb_2O_6$-$K_{0.75}Na_{0.25}NbO_3$ are also being studied for their optical, nonlinear optical, pyroelectric and millimeter wave properties.

3.2 Electro-Optic Character and Importance of T.B. Crystals

For all oxygen octahedron structure materials which are primary candidates, the linear electro-optic effect in the ferroelectric single domain can be traced to a spontaneous polarization-biased quadratic response of the paraelectric prototype, i.e.,

$$\Delta B_{ij} = g^x_{ijrs} P_{r(sp)} n^x_{sk} E_k = r^x_{ijk} E_k \qquad (3.1)$$

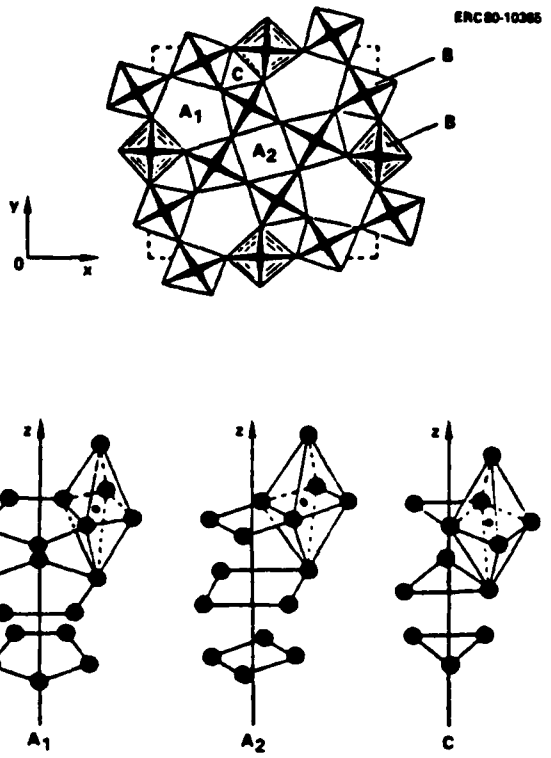

Fig. 1 Projection of structure of tetragonal tungsten bronze parallel to [001].

where

ΔB_{ij} = the incremental change in the optical permeability tensor

E_k = the applied field

r^x_{ijk} = the clamped electro-optic coefficient

g^x_{ijrs} = the quadratic electro-optic constant in the prototypic paraelectric state

$P_{r(sp)}$ = the spontaneous polarization vector in the ferroelectric single domain

n^x_{sk} = the clamped dielectric susceptibility.

From the polarization potential theory of DiDominico and Wemple,[3] the g coefficients depend dominantly on the BO_6 octahedron and change little across a very wide family of perovskites, bronzes and other octahedron-based oxide ferroelectrics. Perhaps the only exceptions are structures containing highly polarizable cations such as Pb and Bi. Clearly from Eq. (3.1), the major concern is to achieve simultaneously high values of $P_{r(sp)}$ and n_{sk}^{x}. The tungsten bronze family materials have the following advantages over the perovskites:

1. This family of crystals possesses extraordinarily large transverse and longitudinal electro-optic coefficients, especially near a morphotropic phase boundary (MPB).

2. Trade-off between sensitivity and speed can be investigated for photorefractive studies due to the structural flexibility. In the tungsten bronze structure, several crystallographic sites are partially empty, which allows the composition to be tailored.

3. Several ferroelectric MPB compositions have now been identified.

4. The lower prototytpe symmetry gives a large family of g constants (quadratic and electro-optic) and the possibility of anisotropic conduction. The nonzero values are g_{11}, g_{12}, g_{13}, g_{44} and g_{66}, as compared to g_{11}, g_{12} and g_{44} in perovskites.

5. In the tetragonal bronzes, since the prototype symmetry is 4mm, only one unique 4-fold axis exists and 90° twins are absent; hence crystals are not likely to crack during poling as reported for $BaTiO_3$.

3.3 Material Growth Techniques

Most of the bronze compositions grown in our laboratory are based on solid solution systems; therefore suitable growth techniques to produce crystals free of optical defects such as striations, scattering centers and twinning must

be developed. Striations and other defects are typical problems common to solid solution crystals, and it is often difficult to suppress them completely. However, these problems can be reduced effectively such that the crystals can be useful for optical device studies. The difficulty of this task underscores the criticality of selecting appropriate growth techniques in the present work. At present, three different techniques have been chosen to develop these bronze crystals. They are as follows:

1. Bulk Single Crystals: Czochralski technique
2. Strip Crystals: Edge defined film-fed technique
3. Thin Films: Liquid phase epitaxy (LPE)

The first two techniques are well established in our current work, and bulk crystals and films of BSKNN-1 and BSKNN-2 compositions have already been grown. In the present report, the continued growth of good quality BSKNN bulk and strip crystals is discussed along with associated growth problems.

3.3.1 Single Crystal Growth Procedure

Nb_2O_5, $SrCO_3$, Na_2CO_3, CeO_2, K_2CO_3 and $BaCO_3$ fine powders have been used as starting materials and have been weighed out in the desired proportions, as summarized in Table 1. The batch mixture is ball-milled in acetone for 20-30 h, and then is poured into a large drying dish. The dried powder is placed in a platinum reaction dish and is calcined at 1000°C for 10-15 h to eliminate carbonates and any possible carbon from the pyrolytic breakdown of residual acetone. The calcined powder is then ball-milled and refired in an oxygen flow of 2 cfh at 1250°C for about 4-6 h. Phase checks and x-ray lattice constant measurements are made for each batch to ensure the use of a phase-pure bronze composition for crystal growth. A thick-walled platinum crucible (2 × 2 in.) is used for this growth, and this container holds roughly 450 g of melt composition.

Table 1

Materials for BSKNN-1 and BSKNN-2 Bulk Single Crystal Growth

Crystal Composition	Starting Materials		Conditions and Remarks
BSKNN-1	• $BaCO_3$	78.93 g	• Congruent melting (1430°C)
	• $SrCO_3$	39.60 g	• Moderate size crystals (0.5 to 1.0 cm)
	• Na_2CO_3	4.41 g	• Large r_{51}, d_{15}, ε_{11}
	• K_2CO_3	20.33 g	• Crack-free
	• Nb_2O_5	221.00 g	
	Total	364.27 g	
Ce-Doped BSKNN-1	• BSKNN-1	364.27 g	• Crack-free crystals
	Ce	1.05 g	• Moderate size crystals (0.5 to 1.0 cm)
BSKNN-2	• $BaCO_3$	33.00 g	• Congruent melting (1450°C)
	• $SrCO_3$	73.66 g	• Moderate size crystals (1.0 to 1.5 cm)
	• Na_2CO_3	8.75 g	
	• K_2CO_3	13.43 g	• Large r_{51}, d_{15}, ε_{11}
	• Nb_2O_5	221.00 g	• Crack-free
	Total	350.0 g	

3.3.2 Czochralski Growth of BSKNN Crystals

The compositions $Ba_{1.2}Sr_{0.8}K_{0.75}Na_{0.25}Nb_5O_{15}$ (BSKNN-1) and $Ba_{0.5}Sr_{1.5}K_{0.5}Na_{0.5}Nb_5O_{15}$ (BSKNN-2) which are being developed under this program exist on the quaternary $BaNb_2O_6$-$SrNb_2O_6$-$KNbO_3$-$NaNbO_3$ system. Figure 2 shows the phase diagram for this quaternary system, and it is seen that the tungsten bronze solid solution exists over a wide compositional range. Both

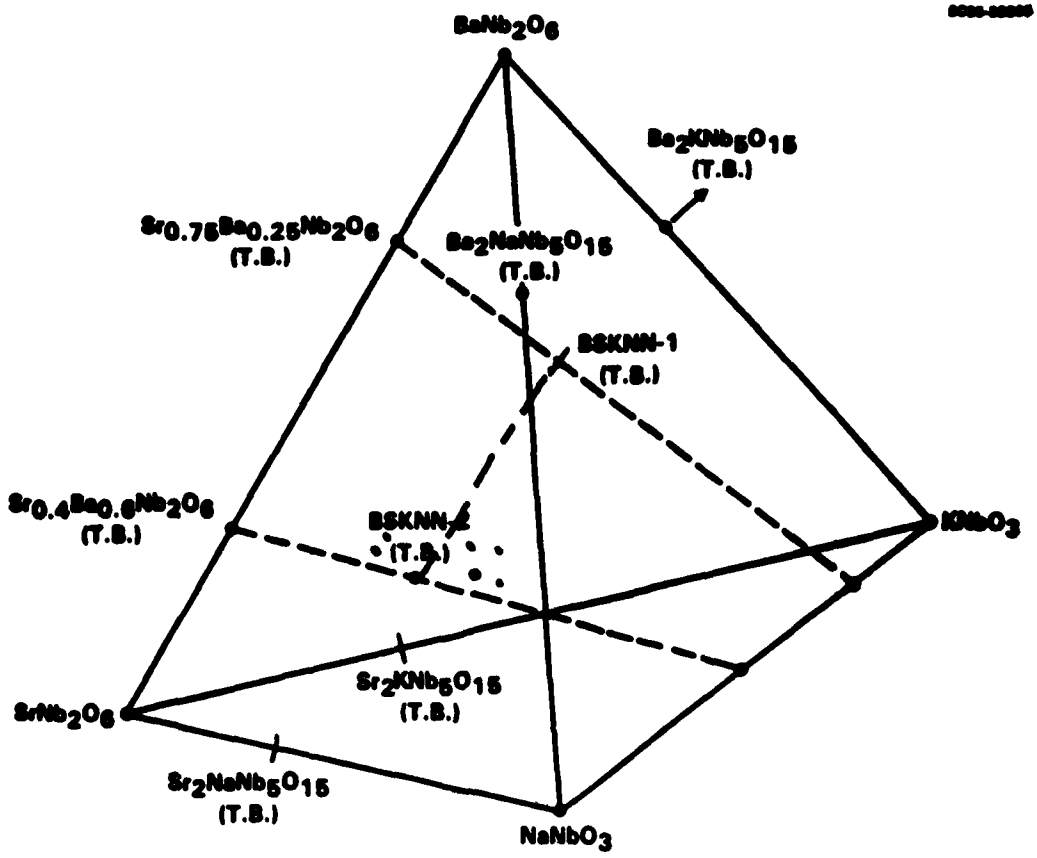

Fig. 2 Quaternary phase diagram for the $BaNb_2O_6$-$SrNb_2O_6$-$KNbO_3$-$NaNbO_3$ system. Shaded area is tetragonal tungsten bronze.

orthorhombic phases, e.g., $Ba_2NaNb_5O_{15}$, $Sr_2NaNb_5O_{15}$, etc., and tetragonal phases, e.g., $Ba_2KNb_5O_{15}$, $Sr_{1-x}Ba_xNb_2O_6$, etc., have been identified for this solid solution. The BSKNN-1 and BSKNN-2 phases were studied on the basis of the pseudo-binary systems $Sr_{0.3}Ba_{0.7}Nb_2O_6$-$K_{0.75}Na_{0.25}NbO_3$ and $Sr_{0.75}Ba_{0.25}Nb_2O_6$-$K_{0.5}Na_{0.5}NbO_3$, respectively. Because of the complexity of the phase diagram, it is often difficult to establish true congruent melting compositions for such a multicomponent system; hence striations and other optical defects can occur for such crystals. However, these problems can be reduced effectively so that the crystals can be useful for optical device studies.

The Czochralski technique is now well established for these compositions, and crystals of reasonable quality and size are being produced. Figure 3 shows typical BSKNN-1 and BSKNN-2 crystals grown along the c-axis. These crystals are a little over 1 cm in diameter; this is the first time such large crystals of these compositions have been grown. During the last year, a considerable effort was also made to improve crystal quality using an automatic diameter control system. The present improvements in BSKNN crystal quality and size have primarily resulted from the control of the following factors which affect crystal growth:

1. Reduction of Nb^{5+} to Nb^{4+} at the growth temperature, if oxygen pressure is low. Nb^{4+} acts as an impurity.

2. Presence of impurity ions, e.g. Ca^{2+}, Fe^{3+}, Na^{+} and Mg^{2+} etc., in the starting materials.

3. Temperature fluctuations at the growth temperature, if growth is conducted without a post-annealing furnace.

4. Pulling and rotation rates are found to affect the presence of striations.

All of these problems have been carefully studied and we have found that the growth of reasonable quality crystals is possible by reducing or eliminating them. Of these, the maintenance of temperature stability is a very difficult task and is considered to be essential for future growth work. Recent phase diagram work on these two pseudo-binary BSKNN systems has shown that the current BSKNN-1 composition is close to congruent melting, and hence improved temperature stability should yield striation-free BSKNN crystals. In order to successfully accomplish this task, several modifications will be made in the growth experiments:

SC85-34226

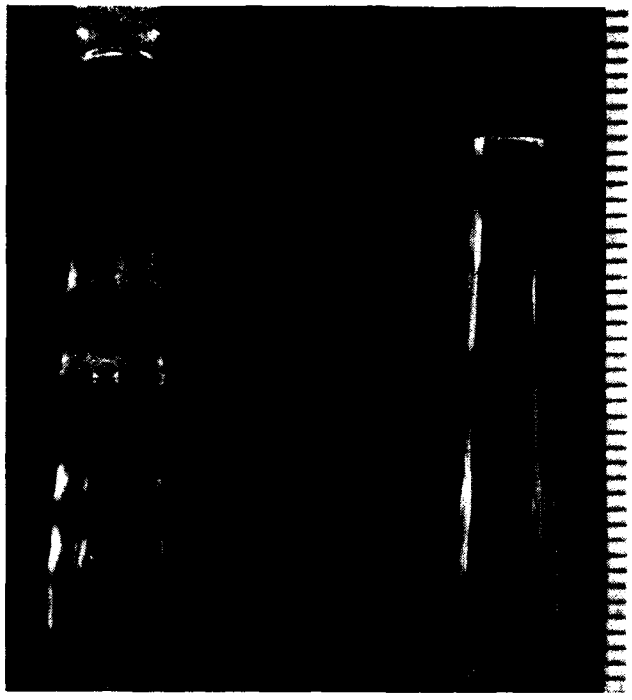

BSKNN II
NO. 162

BSKNN I
NO. 131

Fig. 3 Undoped BSKNN-1 and BSKNN-2 crystals grown along the c-axis.

1. Redesign the post-annealing furnace conditions for this growth in order to achieve a higher order of temperature stability.

2. Use large crucibles and pull small crystals (~ 1 to 1.5 cm in diameter) to minimize compositional gradients.

3. Effectively use the automatic diameter control system to minimize compositional gradients and improve temperature stability.

The automatic diameter controller is in service and allows us to maintain uniform crystal size and weight and enables us to maintain a sufficient temperature stability of ± 2°C; however, we are trying to improve it to ± 1°C or better. It is expected that by achieving improved temperature stability and true congruent melting compositions within the BSKNN system, there is a good possibility of obtaining striation-free, low defect BSKNN bronze crystals for optical device applications.

3.3.3 Controlled Cross-Section Growth of BSKNN Crystals

Recently a new technique known as "controlled cross section" growth was introduced in our ferroelectric materials development programs to develop high optical quality bronze crystals from the BSKNN-1 composition. The process is quite similar to the Czochralski technique except that the crystals are pulled without rotation. This has proven to be considerably successful in pulling crystals of good optical quality with weak or almost absent striae. As shown in Fig. 4, dimensions so far achieved are approximately 1 cm in width, with length limited only by the pulling mechanism or melt volume. Growths in other directions such as (100) and (110) have also been tried and are found to be suitable in developing completely striation-free crystals. This is a significant accomplishment and this technique is being extended to other equally important bronze compositions. The potential of this novel technique has not yet been fully utilized in the area of optoelectronic materials. The improvements in material quality and physical properties, including electro-optic, dielectric and piezoelectric, of bronze materials such as BSKNN through this novel growth technique have exciting potential for important scientific and technological impact.

The growth of crystals pulled with no rotation is more difficult than normal growth, but recently the technique was simplified by using an asymmetrical furnace geometry, since radial thermal gradients must be controlled and must also be well centered on the crystallization axis. BSKNN-1 crystals pulled under these conditions are of excellent optical quality and also show

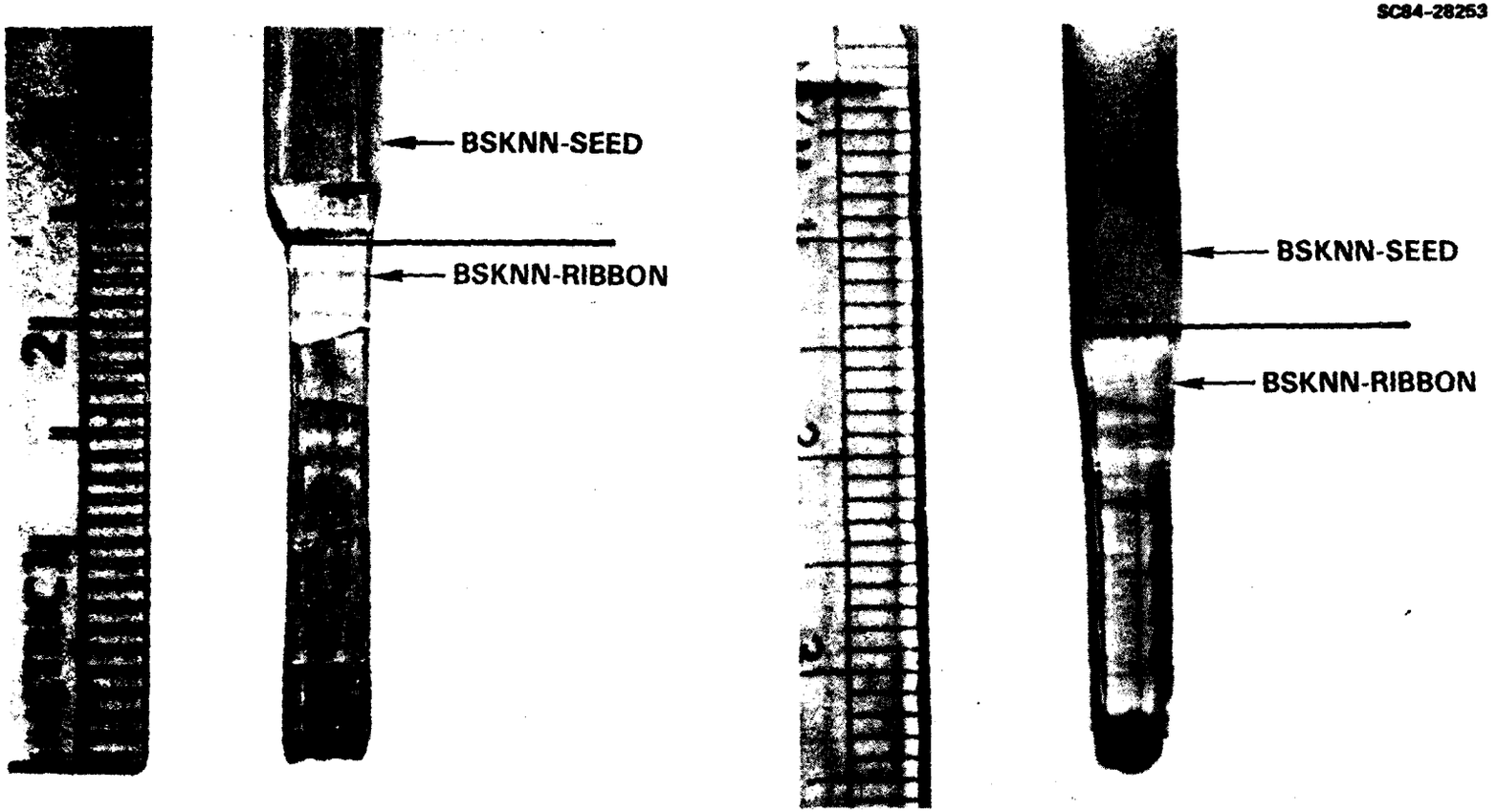

a) BSKNN RIBBON = EXHIBIT STRIATIONS

b) BSKNN RIBBON = EXHIBIT MINIMUM STRIATIONS

Fig. 4 Controlled cross-section growth of BSKNN-1 ribbon crystals.

minimum or no striations. Another important factor to the success of this method is the ability to pull crystals without the occurrence of spontaneous nucleation. This requires that the melt composition should have a low viscosity with a high supercooling range at the growth temperature. Our current $Ba_{1.2}Sr_{0.8}K_{0.75}Na_{0.25}Nb_5O_{15}$ composition is close to congruent melting and has sufficiently low viscosity, and is an excellent candidate for this type of growth. Further improvements in this growth technique should allow us to develop still better quality BSKNN crystals.

3.3.4 LPE Growth of BSKNN Thin Films

The LPE growth technique can be used when crystal growth and quality are difficult to achieve by the Czochralski technique. The LPE technique is relatively simple and widely used today for preparation of epi-films of diverse magnetic, semiconductor and ferroelectric materials; as such, this method can enhance the development of some bronze compositions for electro-optic studies. The LPE process consists of dipping a polished substrate into a solution which is supersaturated with respect to the compound to be grown. The growth solution is contained in a platinum crucible and is maintained at a precisely controlled growth temperature after being heated to a higher temperature to effect complete solution. When equilibrium has been established, the substrate is slowly lowered into the furnace, held just above the surface of the melt for a few minutes, and then immersed into the solution. After the required time for film growth has elapsed, the sample is withdrawn from the melt.

Crucial to the success of isothermal LPE growth is an ability to supercool the solution without the occurrence of spontaneous nucleation. It is therefore necessary to find a suitable flux system for each chosen bronze composition before LPE growth can be performed. Although a large number of solvents has been identified for this family, for the following reasons we have restricted this work to only vanadium-containing solvents:

1. V^{5+} cation has a strong preference for the 4-fold coordinated site, and hence, no vanadium inclusion in the structure is observed.

2. Supercooling range for the V^{5+}-containing solvents is reasonably high, on the order of 20° to 40°C.

3. V^{5+}-containing solvents melt at relatively low temperatures.

4. All V^{5+}-containing solvents dissolve in water or dilute acids, and film cleaning therefore poses no problems.

Based on our past work on ferroelectric $LiNbO_3$ thin film growth[4-6] and the current work on the bronze compositions,[7] it has been found that the vanadium containing solvents are useful for many bronze compositions. Table 2 summarizes the various solvents studied for the large unit cell bronzes. Although all of these solvents are useful for LPE work, the system KVO_3-BSKNN has been studied in greatest detail since it offers BSKNN films of different compositions. Figure 5 shows the potential LPE growth temperatures from the development of the compositional phase diagram for the KVO_3-BSKNN system, and as can be seen, the single phase BSKNN solid solution extends over a wide compositional range. This allows us to grow films of different compositions, particularly those which have a large electro-optic coefficient for modulators and wave-guide applications.

Successful thin film growth also depends strongly on the lattice match between film/substrate and the availability of substrates for this work. Since we plan to use BSKNN and SBN:50 single crystals as substrate materials, a sufficient supply of these crystals is needed. Currently, BSKNN and SBN:50 single crystals, grown under this as well as DARPA (SBN:50) contracts, have been characterized and limited work on film growth has now been performed.

Table 2

LPE Growth Conditions for Large Unit Cell Bronze Compositions

Composition	Solvents	Growth Temp. (°C)	Supercooling Range (°C)	Unit Cell		Lattice Mismatch (on BSKNN)		Lattice Mismatch (SBN:50)*	
				a_A	c_A	a_A	c_A	a_A	c_A
$Ba_{2-x}Sr_xK_{1-y}Na_yNb_5O_{15}$	KVO_3	900	20-40	12.515	3.982	0.01%	0.02%	0.16%	0.503%
	$NaVO_3$	950	20-30	12.514	3.983	0.01%	0.03%	0.16%	0.503%
$Ba_6Ti_2Nb_8O_{30}$	BaV_2O_6	1000	10-30	12.54	4.01	0.233%	0.753%	0.48%	1.12%
	SrV_2O_6	950	10-20	12.54	4.01	0.233%	0.753%	0.48%	1.12%
$K_3Li_2Nb_5O_{15}$	KVO_3	800	30-50	12.58	4.015	0.55%	0.76%	0.80%	1.230%
	$NaVO_3$	850	20-30	12.58	4.015	0.55%	0.76%	0.80%	1.230%

SBN:50 = $Sr_{0.50}Ba_{0.50}Nb_2O_6$

*Unit Cell for SBN:50 = a_A = 12.46; c_A = 3.96

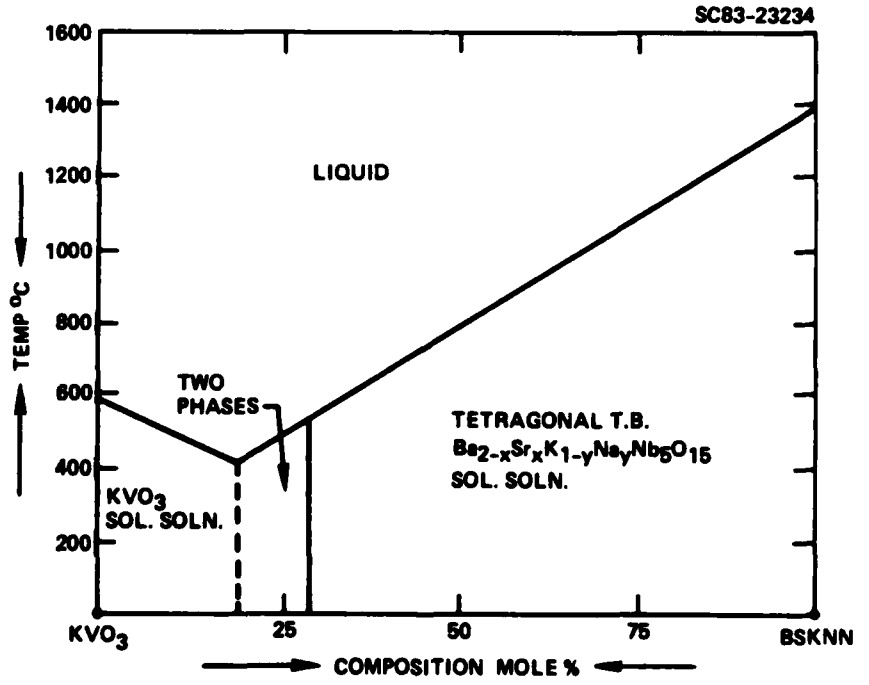

Fig. 5 Partial phase diagram for the KVO_3-BSKNN system.

A mixture containing 65 mole% KVO_3 and 35 mole% BSKNN was selected for BSKNN film growth since it melts at a relatively low temperature (730°C) and has been found suitable to develop thin films. The LPE apparatus consists of a vertical furnace which can be controlled with an accuracy of ± 1/2°C. The mixture was kept heated overnight at 1050°C and, after achieving complete homogeneity, the molten solution was slowly cooled to the growth temperature (around 730°C) at a rate of 10°C/h. The (100)- and (001)-oriented BSKNN substrates, approximately 3 × 3 mm or smaller, were positioned slightly above the melt in order to equilibrate with the solution temperature, and then dipped into the melt. Using such small substrates, we successfully demonstrated that epilayers of BSKNN compositions can be grown. Furthermore, it was found that the rate of crystallization was much faster along the (001) direction as compared to the (100) direction. A similar behavior has also been observed for bulk single crystal growth of the same composition.

Although the quality and surface properties of these BSKNN films need to be considerably improved before they can be evaluated for optical and ferroelectric properties, it is evident that the LPE growth of these films using a KVO_3 flux is now possible, and therefore this work should be continued. Since bulk single crystals of the compositions BSKNN-1, BSKNN-2 and SBN:50 are becoming available, we anticipate no major problems in future growth work. The development of these ferroelectric films should significantly impact several device applications:

- Optical waveguides and modulators
- Spatial light modulators
- Integrated optics and switching

3.4 Characterization

Czochralski and edge-defined BSKNN bulk crystals appear to be of excellent quality and are clear and transparent. Most of the BSKNN-1 and BSKNN-2 crystals are colorless and are usually well faceted, which is quite

exceptional for Czochralski-grown crystals. The bigger unit cell BSKNN crystals are square in shape and show 4 well-defined facets. On the other hand, smaller unit cell bronzes, e.g., SBN:50, SBN:60, SKN, etc., are cylindrical in shape and exhibit 24 well-defined facets. Figure 6 shows the idealized forms for these crystals. These facets provide a unique advantage for this family, since they can significantly ease the task of crystal orientation.

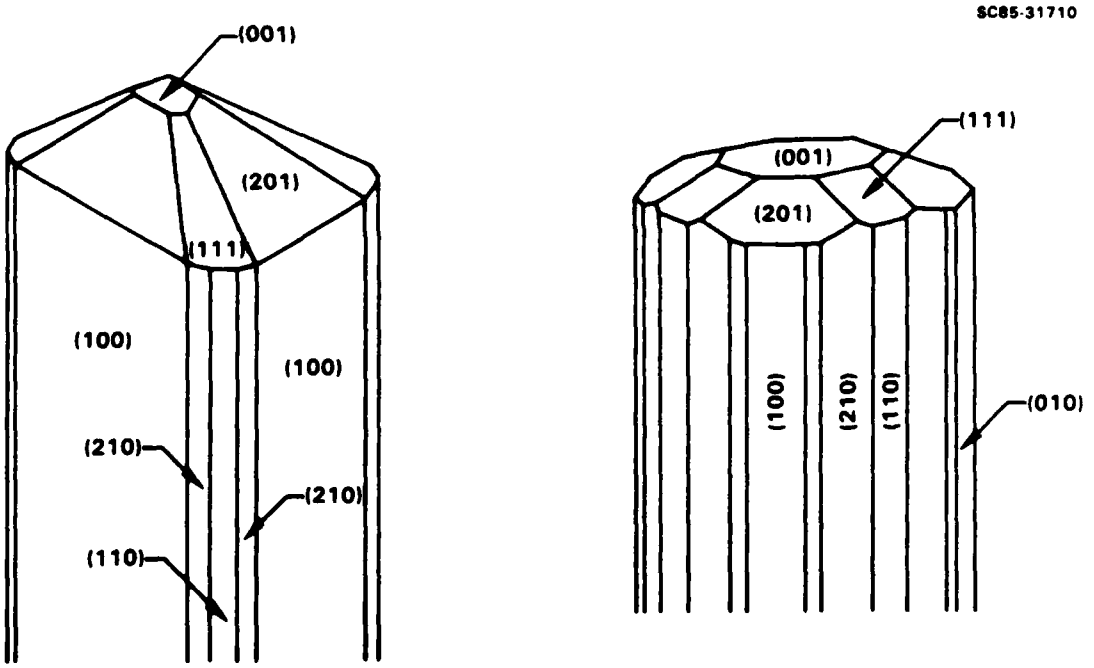

Fig. 6 Partial phase diagram for KVO_3-BSKNN system.

Due to the large number of parameters needed to fully characterize the BSKNN system, which includes 6 elastic, 3 piezoelectric, 3 electro-optic and 2 dielectric, several specimens with various shapes and orientations were used (Fig. 7). Prior to measurement, the crystals were poled by a field-cooling method under a dc field of 10 kV/cm along the (001) direction. The samples were heated to just above the Curie temperature, at which point the field was applied and the samples slowly cooled. In general, sputtered Au or Pt electrodes were used, and the samples were poled in a silicon oil bath (diffusion pump oil), although SBN can also be poled in dry N_2 or O_2. The procedures for determining elastic and piezoelectric constants were similar to those described by Berlincourt and Jaffe[8] utilizing a resonance-antiresonance transmission method. Dielectric constants were measured on (001) and (100) square plates at 1, 10 and 100 KHz using a Hewlett-Packard automatic capacitance bridge. Thermal expansion coefficients ($\varepsilon_1$and ε_3) were determined using high temperature x-ray diffraction measurements. Results of these measurements are not complete and work is in progress to establish this information. These data are not only useful for optical applications, but also are very important for LPE growth work.

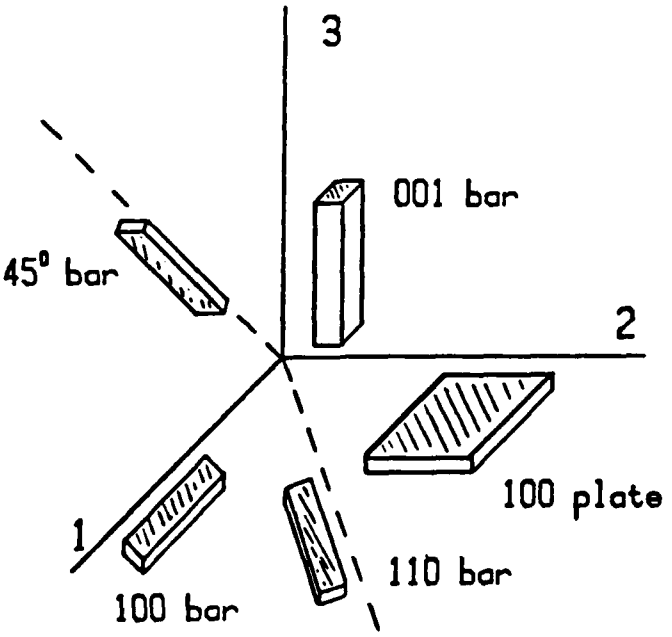

Fig. 7 Shapes and orientations of test specimens.

The spontaneous polarization (P_s) as a function of temperature was determined statically. An electrically poled sample, equilibrated at some temperature $T < T_c$, was thermally depoled by quenching in a 200°C silicon oil bath while charge was collected using an electrometer. The piezoelectric strain coefficients d_{33} and f_{15} were measured using a Berlincourt d_{33} meter. The electro-optic coefficients (r_{33} and r_{51}) were measured directly and also from d_{33} and polarization behavior. Table 3 summarizes the various measured ferroelectric constants for BSKNN-1, BSKNN-2 and some other important bronze compositions.

The temperature dependence of the dielectric constants and dielectric loss was measured from 20 to 500°C, depending upon the Curie temperature, T_c, for the given crystal. Both ε_{33} and ε_{11} showed marked anomalies at the transition temperature for BSKNN-1 and BSKNN-2 crystals. The general temperature behavior and large anisotropy of ε_{33} and ε_{11} are typical of all bronze crystals. However, the magnitude of the room temperature dielectric constant is markedly different for each composition, and seems to depend strongly on the size of the unit cell of the given bronze crystal. For example, ε_{11} is large while ε_{33} is small for the bigger unit cell bronzes, e.g., BSKNN-1, PBN and KLN. On the other hand, the situation is reversed in the case of smaller unit cell bronzes where ε_{33} is larger while ε_{11} is smaller. The dielectric constants were further studied by cooling below room temperature, and it was found that in the case of bigger unit cell bronzes, the dielectric constant ε_{11} increases with decreasing temperature, indicating the presence of another ferroelectric-ferroelastic phase transition. Toledano et al[9] also reported this type of behavior for another bronze crystal, $Ba_2NaNb_5O_{15}$. Further work is in progress on bigger unit cell BSKNN-1 and KLN crystals to confirm the existence and location in temperature of these low temperature transitions. In general, the dielectric loss for these crystals is on the order of 0.03 or less at room temperature.

Other ferroelectric properties, such as the piezoelectric strain coefficients, are also reversed when going from bigger unit cell to smaller unit cell bronzes. For example, d_{15} is larger while d_{33} is smaller for

Table 3

Physical Properties of Tetragonal (4mm) Bronze Crystals

Structure		BSKNN-2	BSKNN-1	SBN:60	SBN:75
T_c (°C)		175	209	78	56
Lattice Constants (A)*	a	12.4799	12.510	12.469	12.447
	c	3.9471	3.980	3.938	3.929
Density (g/cc)		5.6	5.14	5.21	5.19
Spontaneous Polarization P_s (C/m^2)*		0.30	0.28		
Pyroelectric Coeff (p) (10^{-4} C/m^2-K)		4.3	-	8.5	-
Dielectric constants	ε_{11}	850	380	900	3400
	ε_{33}	250	180	400	-
Piezoelectric Coeff (10^{-12} C/N)	d_{15}	118	70	24	-
	d_{31}	-28	-	-110	-
	d_{33}	75	60	120	130
Piezoelectric Coupling Coeff	k_{15}	0.37	0.38	0.24	-
	k_{31}	0.18	-	0.14	-
	k_{33}	0.49	0.46	0.47	-
	k_p	0.29	-	0.21	-
	K_t	0.41	-	0.44	-
Electro-Optic Coeff (10^{-12} m/V)	r_{51}	> 380	> 380	80	60
	r_{33}	> 380	380	420	1400

*All crystals are tetragonal with 4mm point symmetry.

BSKNN-1 and KLN. On the other hand, d_{33} is larger while d_{15} is smaller for SBN, SKN, etc. These piezoelectric properties are of particular importance for electro-optic applications since the d_{ij} and r_{ij} coefficients are related. This may be seen from the phenomenological equations for the tetragonal phases as, for example,

$$d_{15} = Q_{44}\varepsilon_{11}P_3 \quad , \tag{3.2}$$

where Q is the quadratic shear electrostriction constant in the paraelectric (4/mmm) prototype and P is the spontaneous polarization, and

$$r_{51} = g_{44}\varepsilon_{11}P_3 \tag{3.3}$$

where g is the quadratic electro-optic constant of the prototype. The Q and g constants are found to vary only slightly across a wide range of bronze compositions, and are largely independent of temperature. Therefore, the d and r coefficients are expected to have nearly the same temperature and compositional characteristics, depending in the same manner upon P and the dielectric permittivity, ε. In the case of BSKNN-1, r_{51} has been found to be larger than that for smaller unit cell bronzes, as expected, whereas r_{33} is smaller, depending as it does on ε_{33}. This general difference between the smaller and larger unit cell bronzes classifies the bronze family into two groups, as summarized in Table 4.

The results of birefringence measurements on BSKNN along with those for other tungsten bronzes are shown in Fig. 8. It is significant to note that the composition $Ba_{1.2}Sr_{0.8}K_{0.75}Na_{0.25}Nb_5O_{15}$ has a room temperature birefringence Δn_{31} 2.5 times greater than that for SBN:60. The birefringence is directly related to the electro-optic quadratic g coefficients and the linear r coefficients, and hence the results given in Fig. 8 indicate the strong potential of BSKNN for future electro-optical device applications.

Table 4

Classification of Tungsten Bronze Family

T.B. Compositions with Smaller Unit Cell Dimensions	T.B. Compositions with Larger Unit Cell Dimensions
e.g., $Sr_{1-x}Ba_xNb_2O_6$ and $Sr_2KNb_5O_{15}$	e.g., $Ba_6Ti_2Nb_8O_{30}$, $Sr_2Ti_2Nb_8O_{30}$ BSKNN, etc.
• Crystal habit is cylindrical with 24 well-defined facets	• Crystal habit square with 4 well-defined facets
• High electro-optic (r_{33}) and pyroelectric effects	• High electro-optic coefficient (r_{51})
• High delectric constant (ε_{33})	• High dielectric constant (ε_{11})
• High piezoelectric d_{33} coefficient but low d_{15}	• High piezoelectric d_{15} coefficient, but low d_{33}
• Large crystals with excellent quality are available (2-3.0 cm in diameter)	• Moderately large crystals are available (~ 1-1.5 cm)
• Low phase transition temperature (below 150°C)	• High phase transition temperature (above 150°C)

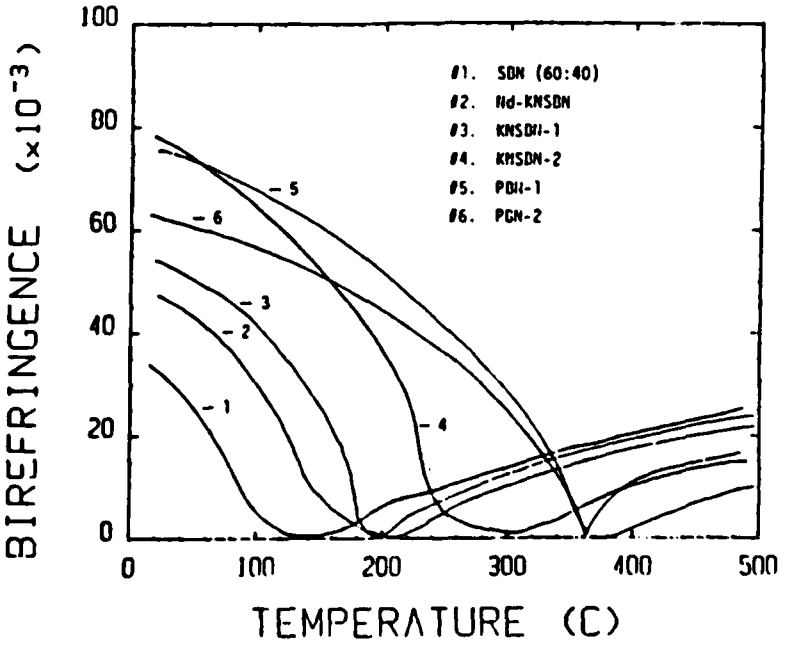

Fig. 8 Birefringence Δn_{31} vs temperature for various tungsten bronzes.

The availability of these crystals has opened up a variety of new device concepts which includes electro-optic, photorefractive, pyroelectric, SAW, millimeter wave and transduce applications. Figure 9 shows a number of device concepts being explored at Rockwell using both bronze crystals and ceramics. In each case, significant progress has been made.

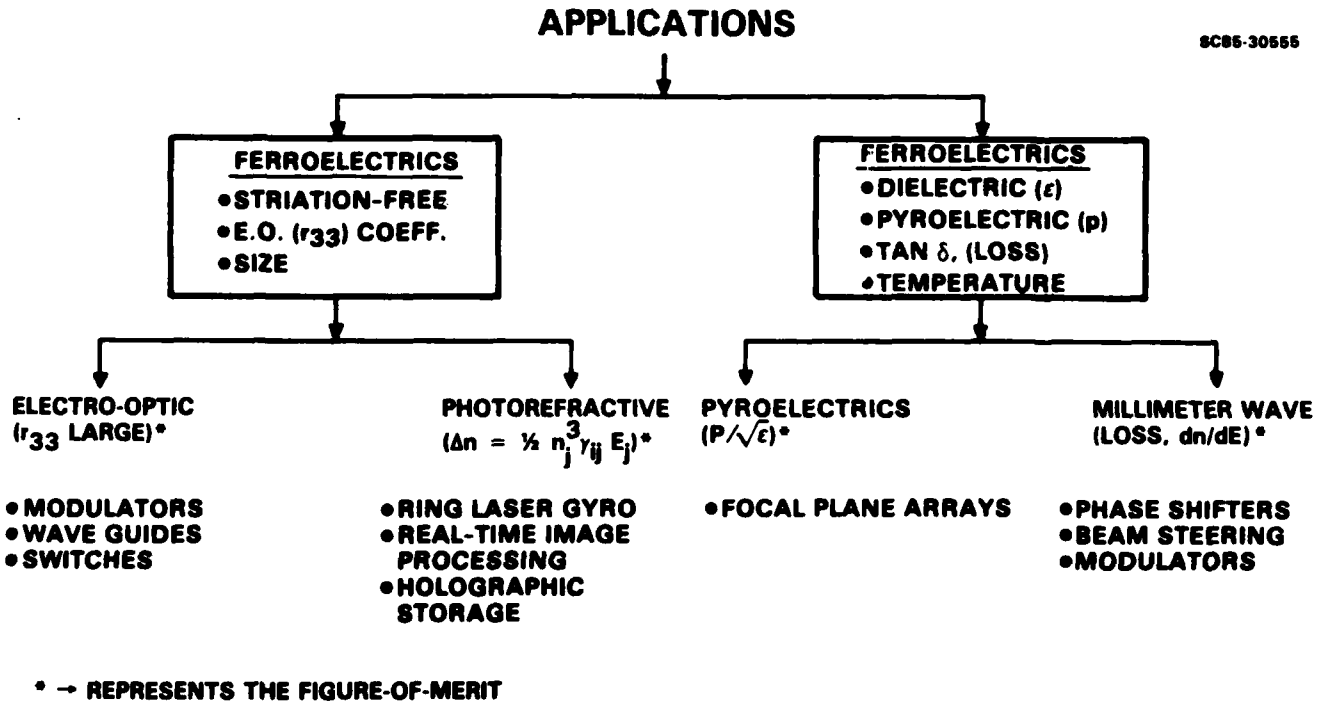

Fig. 9 Applications of ferroelectric tungsten bronze crystals.

4.0 DOPED BSKNN CRYSTALS FOR PHOTOREFRACTIVE STUDIES

4.1 Introduction

The term photorefractive effect has been adopted to refer to optically induced changes of refractive index which occur in many spontaneously polarized materials. This effect has recently been employed for optical storage of information by holographic technology and for real time image processing using four-wave mixing. These devices require a suitable material that possesses high photorefractive sensitivity with short response time. At present, no single material combines all these features; hence, a large number of ferroelectric crystal compositions have been grown and characterized to establish a possible trade-off between sensitivity and speed. Nonferroelectric $Bi_{12}SiO_{20}$ (BSO) crystal has the desired response time, but its photorefractive sensitivity is poor. On the other hand, all other ferroelectric materials such as $LiNbO_3$, $LiTaO_3$, $KNbO_3$, $BaTiO_3$, $KTa_{1-x}Nb_xO_3$ (KTN), $Ba_2NaNb_5O_{15}$, $Sr_{1-x}Ba_xNb_2O_6$ (SBN), etc., possess high photorefractive sensitivity, but moderate response times. This is a key issue in this work, and attempts are being made using ferroelectric tungsten bronze BSKNN and other suitable crystals to improve the response time without compromising efficiency. The major advantages of the bronze family crystals are as follows:

- Tungsten bronze family crystals possess very high electro-optic coefficients.
- Large size (over 1 in. in diameter) and optically good quality crystals are available, e.g., SBN, BSKNN, PBN, SKN, etc.
- The open structure of the tungsten bronzes will accommodate wide range of single or multiple dopant species.
- Compositional flexibility permits modification of refractive index and other key properties of the host.

A significant advance in the technology of ferroelectric materials was achieved with the growth of large sized tungsten bronze crystals such as SBN:60, SBN:50 (over 2.3 cm in diameter), BSKNN (1.5 cm), PBN (1 cm) and SKN (~ 1 cm) at the Rockwell International Science Center. These crystals were developed under DARPA and other sponsorship for use in temperature compensated SAW filters and millimeter wave applications. However, SBN and BSKNN compositions are also very attractive for electro-optic, photorefractive and pyroelectric applications. Furthermore, since the tungsten bronze structure is open and contains five crystallographic sites, namely 15-, 12-, 9-, and two 6-fold coordinated sites, the compositional versatility in this structure should permit a wide range of modifications to adjust the trade-off between sensitivity and speed. This is a unique advantage of this family and makes it superior for many photorefractive applications.

4.2 Growth of Doped BSKNN Crystals

The photorefractive effect in electro-optic materials has been defined as follows

$$\Delta n = -1/2\, n^3 r_{ij} E_j \qquad (4.1)$$

where r = electro-optic coefficient

n = refractive index

E = space charge field.

From this equation it is clear that, for the best performance, the electro-optic coefficient and space charge field should be large. Furthermore, the space charge field should develop quickly compared to the required response time in various device applications. For a given electro-optic material, one seeks to maximize both sensitivity and speed. The photorefractive sensitivity of these materials is defined by Glass, et al[10] as:

$$S = \frac{\Delta n}{dW} \quad , \tag{4.2}$$

where $W = \int I dt$ is the incident energy density.

Since the electro-optic coefficients (e.g., r_{51}) are more or less constant for the BSKNN-1 composition, improvements in both photorefractive sensitivity and speed are being studied using various dopants such as Fe^{2+}/Fe^{3+}, Ce^{3+}/Ce^{4+}, Mo^{4+}/Mo^{6+}, Ce^{3+}/Fe^{3+} etc. The role of Ce and Fe cations has recently been studied in SBN:60 crystals, and initial efforts will now concentrate on these impurities in BSKNN to establish their site preference, distribution (over different crystallographic sites) and valance states, along with their influence on sensitivity and speed. Using these results, it will be possible to explore other suitable impurity species in this composition and will also enable the development of a suitable model to determine the influence of ferroelectric characteristics and the role of impurity ions in controlling the photorefractive properties.

The addition of Ce in SBN:60 seems to favor the improvement of both sensitivity and speed; hence, Ce-doped BSKNN-1 crystals have been grown in the present study. The concentration of Ce in BSKNN is close to 0.1 wt% and for this addition the growth conditions did not change appreciably. Figure 10 shows a typical Ce-doped BSKNN-1 crystal growth along the (001) direction. This crystal is almost 1.5 cm in diameter and crystal quality is reasonable. The addition of Ce in BSKNN did not change the striation pattern and it is believed that further improvements in our starting materials and temperature control during growth should result in the development of optical quality crystals.

The Ce-doped BSKNN-1 crystals are pink in color and show four well-defined facets. The Curie temperature and dielectric constant were determined for this composition using standard dielectric measurement techniques. The Curie temperature reduced from 209° to 200°C for this addition, while the dielectric constant slightly increased, indicating a similar enhancement in electro-optic properties. Currently, we are trying to establish both the

SC84-28252

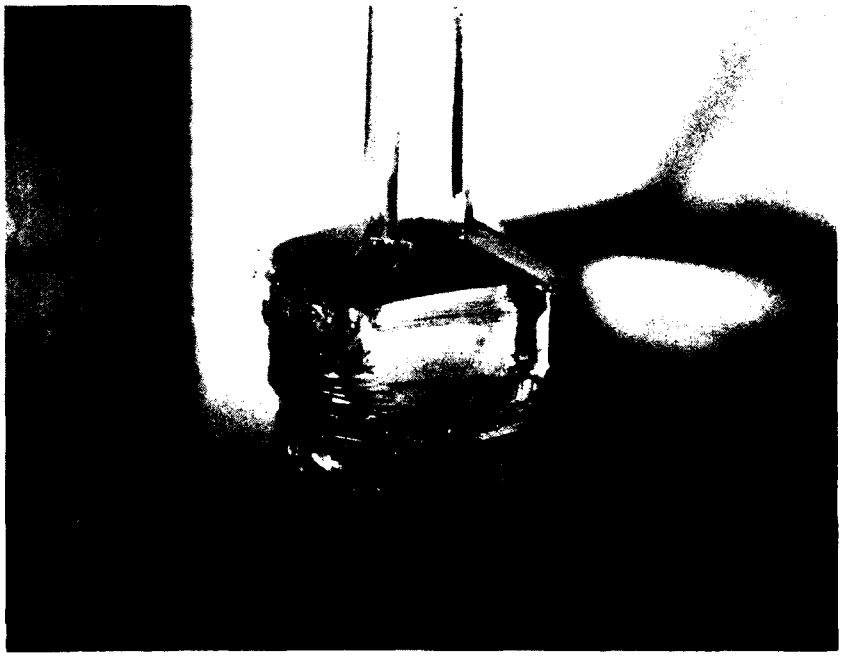

Fig. 10 Ce-doped BSKNN-1 crystals grown along the [001] direction.

photorefractive sensitivity and speed for this composition. Since the crystal quality is presently not adequate for determination of all photorefractive properties, initially only the sensitivity will be established. If this property shows enhancement, then work will commence to improve the optical quality of the material.

As discussed in an earlier section, the BSKNN-2 composition has characteristics similar to $BaTiO_3$. It is therefore important to begin parallel work on the Ce doping in BSKNN-2 crystals. Besides Ce, other impurity species will also be tried in this composition. A summary of these impurity ions and their probable site preference is given below:

Doping Involved at One Crystallographic Site

1. 6-fold coordinated site

   Fe^{2+} + Fe^{3+}, Mn^{2+} + Mn^{3+}, Ti^{3+} + Ti^{4+}, etc.

2. 9-fold coordinated site

   Ni^{2+}, Fe^{2+}, Zr^{4+}, Ti^{4+}, Ce^{4+}, etc.

3. 12- or 15-fold coordinated sites

   Ce^{3+}, Tb^{3+}, Bi^{3+}, Eu^{3+}, etc.

Doping Involved at One or More Crystallographic Sites

1. Fe^{2+}, or Mn^{2+} in 6- or 9-fold coordinated site.

2. Ce^{3+} or Tb^{3+} in 12- or 15-fold coordinated site.

Initially, all new doping work will be performed on ceramic powders and only the more promising candidates will be selected for crystal growth. Since the Czochralski bulk single crystal growth technique has been successfully established for tungsten bronze compositions at Rockwell, the role of various impurity species should be determined in a reasonably fast time for BSKNN.

5.0 DEVELOPMENT OF MORPHOTROPIC PHASE BOUNDARY MATERIALS

Another alternative approach to the development of improved electro-optic materials is the growth of morphotropic phase boundary (MPB) composition crystals. Near an MPB, the electro-optic, piezoelectric, dielectric and other ferroelectric properties can be exceptionally large and in some systems they are at least 5 to 10 times better than current best known ferroelectric crystals such as SBN:60 and $BaTiO_3$. Several of the more useful tungsten bronze and perovskite systems, summarized in Table 5, show morphotropic phase boundaries near which polarization is large, giving large electro-optic, dielectric and other ferroelectric properties. As shown in Fig. 11, on a binary phase diagram a MPB appears as a nearly vertical line separating two ferroelectric phases. The chemical composition of the boundary remains nearly constant over a wide temperature range up to the Curie temperature. Crystals poled near such boundaries show unique and enhanced electro-optic properties because of the proximity in free energy of an alternate ferroelectric structure. A detailed description of MPB behavior has been provided by Jaffe et al.[11]

Table 5

Ferroelectric Properties at MPB for Tungsten bronze Systems

System		X at MPB	T_c (°C)	Dielectric Constant at R.T.	Electro-Optic Coefficient $\times 10^{-12}$ m/V	Application
(1-x) $PbNb_2O_6$	- (x)$BaNb_2O_6$	0.37	300	-	-	
	+ La^{3+} (2%)		230	1700	420	MW + EO
	+ La^{3+} (6%)		115	3500	780	MW + EO
(1-x) $Pb_{2.5}Nb_5O_{15}$	- (x)$Sr_2NaNb_5O_{15}$	0.75	135	2200	Large	MW + EO
(1-x) $Pb_2KNb_5O_{15}$	- (x)$Ba_2NaNb_5O_{15}$	0.25	255	1340	Large	MW + EO
(1-x) $Ba_2NaNb_5O_{15}$	- (x)$Sr_2NaNb_5O_{15}$	0.60	170	>500	Low	Pyro
(1-x) $Pb_2KNb_5O_{15}$	- (x)$Sr_2NaNb_5O_{15}$	0.70	155	930	Medium	MW + Pyro

MW = Millimeter Wave
EO = Electro-Optic
Pyro = Pyroelectric

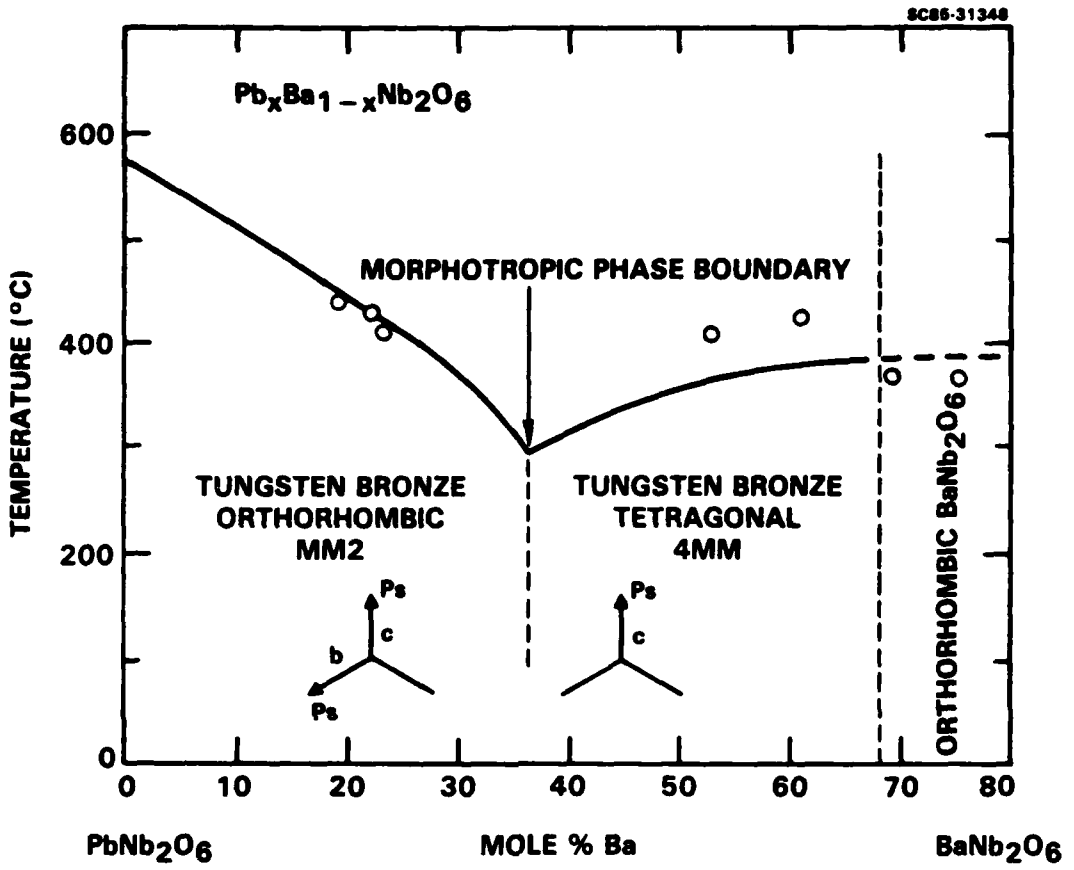

Figure 11 Phase diagram for the $PbNb_2O_6$-$BaNb_2O_6$ system.

In the tungsten bronze $Pb_{1-x}Ba_xNb_2O_6$ system, both tetragonal and orthorhombic phase coexist at x = 0.37. In the tetragonal (4mm) symmetry for ferroelectric bronzes, the electro-optic coefficients r_{ij} of single domains are given from the phenomenological model of Cross and co-workers[12,13] in terms of the g_{ij} quadratic coefficients of the prototype by relations of the form

$$r_{13} = g_{13} P_3 \varepsilon_{33}$$

$$r_{33} = g_{33} P_3 \varepsilon_{33}$$

$$r_{42} = r_{51} = g_{44} P_3 \varepsilon_{11} \qquad (5.1)$$

The last relation is of special interest in that for a composition close to the MPB, but a long way from the ferroelectric Curie temperature, both P_3 and ε_{11} can be very large, and can be largely independent of temperature.

For orthorhombic compositions close to the MPB, the equivalent relations are:

$$r_{11} = r_{22} = 2g_{11}P_1\ \varepsilon_{11}$$

$$r_{12} = r_{21} = 2g_{21}P_1\ \varepsilon_{11}$$

$$r_{13} = r_{23} = 2g_{11}P_1\ \varepsilon_{33}$$

$$r_{34} = r_{35} = 2g_{44}P_1\ \varepsilon_{33}$$

$$r_{16} = r_{26} = 2g_{44}P_1\ \varepsilon_{11} \qquad (5.2)$$

Now it is P_2 and ε_{33} which will be large, so that the anomalously large and nearly temperature invariant values of r_{33} and r_{34} are to be expected.

5.1 PBN System

In the $Pb_{1-x}Ba_xNb_3O_6$ system, we have demonstrated the growth of small crystals (nonoptical quality) close to the MPB. For compositions on both sides of the boundary, the g_{ij} quadratic coefficients are largely temperature independent as expected and are larger than those for SBN. With increasing lead content, the piezoelectric coefficients d_{15} and d_{24} shown in Fig. 12, which are equivalent to r_{51} and r_{42}, escalate dramatically as the composition approaches the MPB and the values are larger than those for $BaTiO_3$. The major advantages of these MPB crystals for photorefractive studies are:

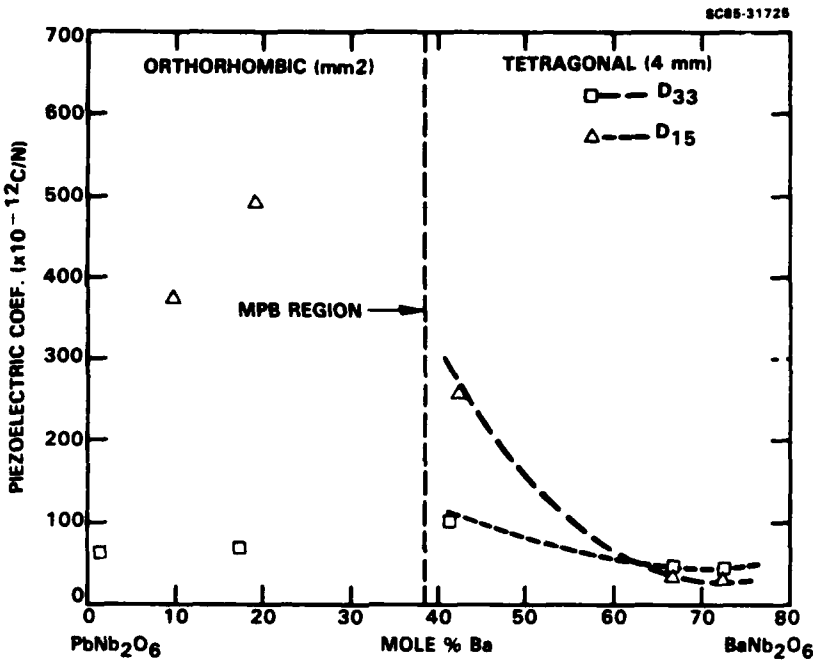

Fig. 12 Piezoelectric behavior of $Pb_{1-x}Ba_xNb_2O_6$ as a function of composition.

1. The separation from phase boundary is a function of composition, not temperature, i.e., the boundary is morphotropic, so that the very high values of the constants persist over a wide temperature range.

2. For compositions close to the boundary, r_{51} and r_{42} values larger than those for $BaTiO_3$ are possible.

3. Since the prototype symmetry is 4/mmm, only one unique 4-fold axis exists, and 90° twins are not possible; hence cracking is not as severe a problem as reported for $BaTiO_3$.

4. Very large transverse drift fields can be achieved.

Although small MPB $Pb_{1-x}Ba_xNb_2O_6$ crystals have been grown, their optical quality is not yet suitable for electro-optic or photorefractive applications.

5.2 New MPB Systems: PSNN and PKSNN

The initial success in developing morphotropic PBN has led to the investigation of other potential Pb-containing morphotropic phase boundary compositions in the tungsten bronze family. In particular, two such systems $(1-x)Pb_{2.5}Nb_5O_{15}$ - $(x)Sr_2NaNb_5O_{15}$ (PN-SNN, or PSNN) and $(1-x)Pb_2KNb_5O_{15}$-$(x)Sr_2NaNb_5O_{15}$ (PKN-SNN, or PKSNN) have been investigated in normally sintered ceramic form and look to be promising for optical crystal development.

Tungsten bronze PKN has now been extensively studied in this laboratory and elsewhere[14,15] in both ceramic and single crystal form. Although large single crystals of PKN have been grown,[14] compositional homogeneity has been a significant problem because of the usual high volatility of Pb^{2+} at the melt temperature (approximately 1300°C). More recently, hot-pressed PKN ceramics have been investgated which show excellent piezoelectric and electromechanical properties. The present work on PKN has involved the pseudo-binary system (1-x)PKN - (x)SNN in cold-pressed ceramic form in order to determine the presence, if any, of morphotropic phase boundary behavior.

The phase diagram for the PKN-SNN system is shown in Fig. 13. These data were obtained from numerous ceramic samples of varying composition using standard dielectric property measurements over the frequency range 100 Hz-100 kHz. The Curie temperature is found to decrease dramatically from that for PKN (425°C) with increasing SNN substitution, reaching a minimum of 155°C for $0.70 < x < 0.75$. For $x > 0.75$, the transition temperature T_c and Curie-Weiss θ value are seen to diverge, indicative of a change from second to first order phase transition behavior. This is further reflected in the dielectric behavior at T_c, shown in Fig. 14, where the dielectric constant undergoes a significant drop for $x > 0.75$, as expected for first order phase transition behavior. At room temperature, the dielectric constant achieves a local

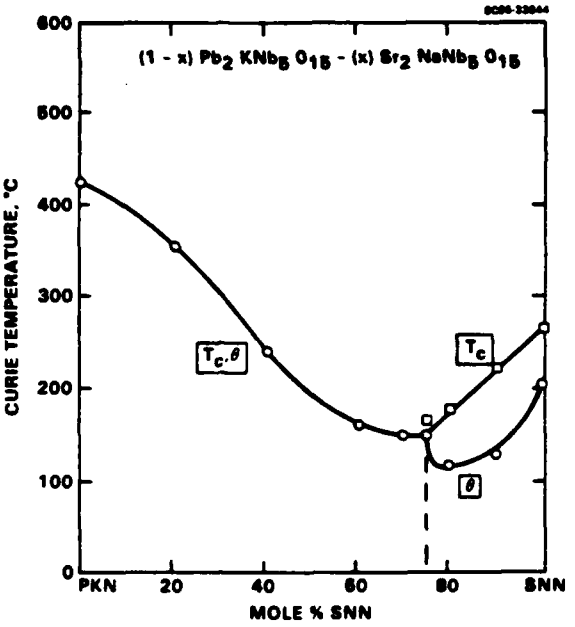

Fig. 13 Phase transition temperature T_c and Curie temperature θ as a function of composition for the PKN-SNN system.

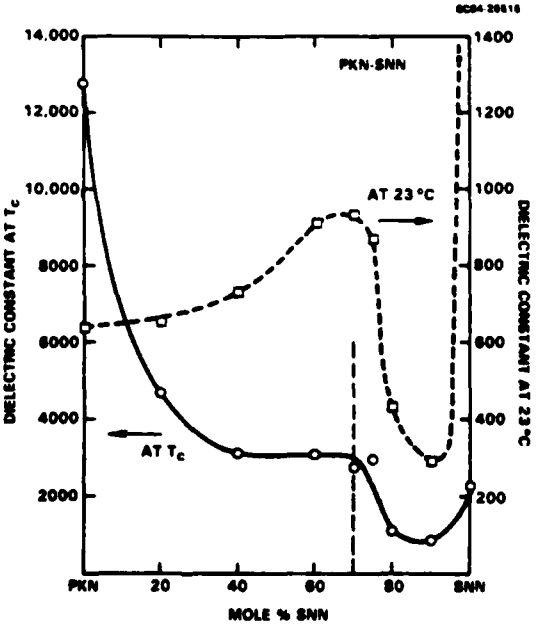

Fig. 14 Compositional dependence of the low frequency dielectric constant for the PKN-SNN system.

maximum near x = 0.70, followed by a precipitous drop for increasing SNN substitution, again indicative of the increasing first order transition behavior. The high room temperature dielectric constant for pure SNN (Fig. 14) is the result of a low temperature phase transition (much less than 0°C) which gives rise to an increasing dielectric constant with decreasing temperature. The Curie-Weiss coefficient C_c decreases from 3.1×10^5 for PKN (similar to SBN) down to 0.8×10^5 for x = 0.70, then rises 1.3×10^5 for pure SNN.

All of the ceramics examined were found to be well sintered in the range 1200-1260°C, with no significant cracking, unlike pure PKN which has been found to have cracking problems for sintering temperatures above 1200°C. Analysis of x-ray powder diffraction measurements shows interesting behavior for the lattice constants in this system, as shown in Fig. 15. Although the system end members, PKN and SNN, respectively show strong and moderate orthorhombic distortion, the structure appears to be essentially tetragonal near x = 0.75 with an indistinguishable difference between the a and b lattice constants. Since the change from orthorhombic to tetragonal or near-tetragonal near x = 0.75 is relatively gradual, it is presently questioned whether this can be called a true morphotropic phase boundary. Nevertheless, the phase transition temperature and dielectric Curie-Weiss behavior as a function of composition are strongly suggestive of a classic morphotropic phase boundary at x = 0.70-0.75. More work is needed to resolve this question; in particular, uncompensated Pb^{2+} losses (2-4% weight loss for 4 h sintering times) may play a role in the apparent gradual behavior of the a and b lattice constants near x = 0.75. Improved sintering with an excess of PbO in the starting mix may also reveal significantly sharper and larger room temperature dielectric behavior in this same compositional region.

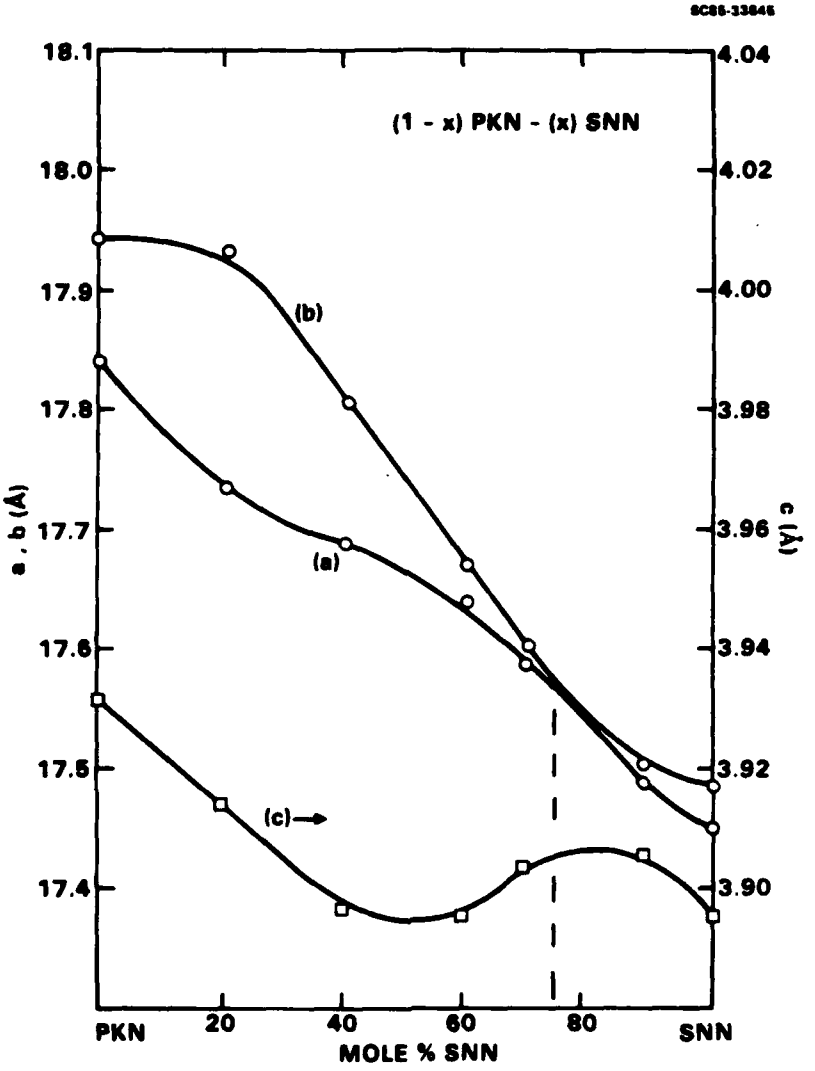

Fig. 15 Compositional dependence of the unit cell lattice constants for the PKN-SNN system.

We have also made an initial examination of another pseudo-binary tungsten bronze system, (1-x)PN - (x)SNN, using normally sintered ceramics. Lead metaniobate (PN) is a widely studied orthorhombic bronze which has already been found to have a morphotropic phase boundary in the $PbNb_2O_6$- $BaNb_2O_6$ system, as discussed earlier in this and previous reports. In the (1-x)PN-(x)SNN system, a morphotropic phase boundary has also been discovered for x = 0.70-0.75, as shown in Fig. 16. The decrease in the phase transition temperature T_c at the MPB is quite dramatic, going from 565°C for pure PN down to 145°C at x = 0.75. The Curie-Weiss behavior is generally first order over the entire

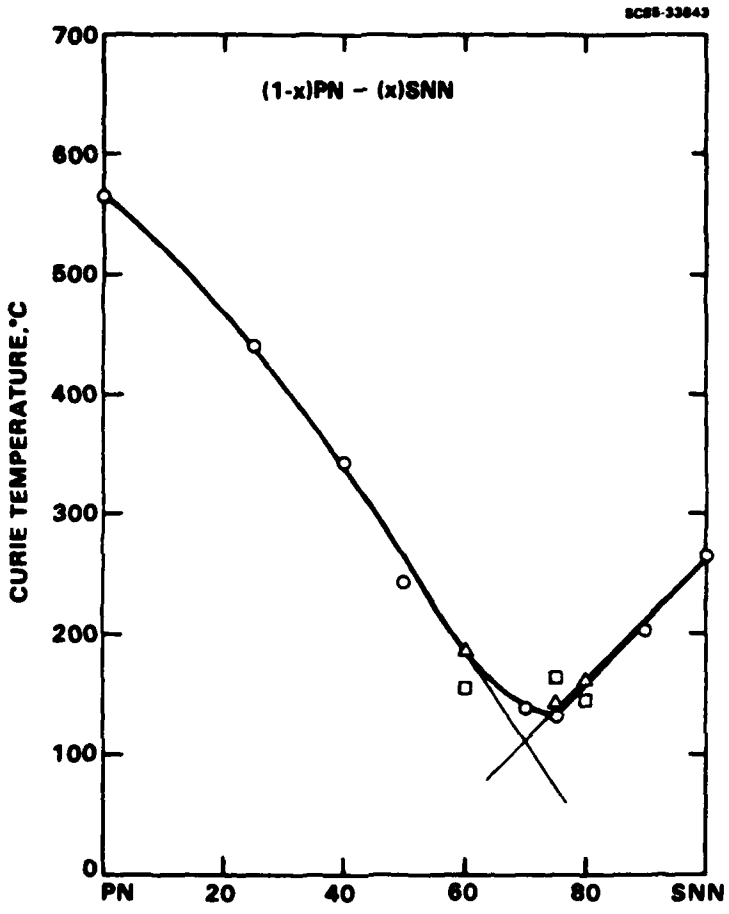

Fig. 16 Phase transition temperature T_c as a function of composition for the PKN-SNN system.

compositional range, with near-vertical dielectric anomalies at the phase transition temperature for highly PN-rich compositions. As shown in Fig. 17, the dielectric peak broadens with SNN substitution, and the room temperature dielectric constant attains a maximum of 3800 at the MPB. It should be kept in mind that the latter value is representative of a normally sintered ceramic; single crystal values could be a factor of 2 or larger, indicating the potential for exceptionally high electro-optic effects. It will be of interest to see whether this orthorhombic/orthorhombic bronze system shows a lattice constant behavior similar to that for PKN-SNN or a more abrupt lattice constant discontinuity at the MPB.

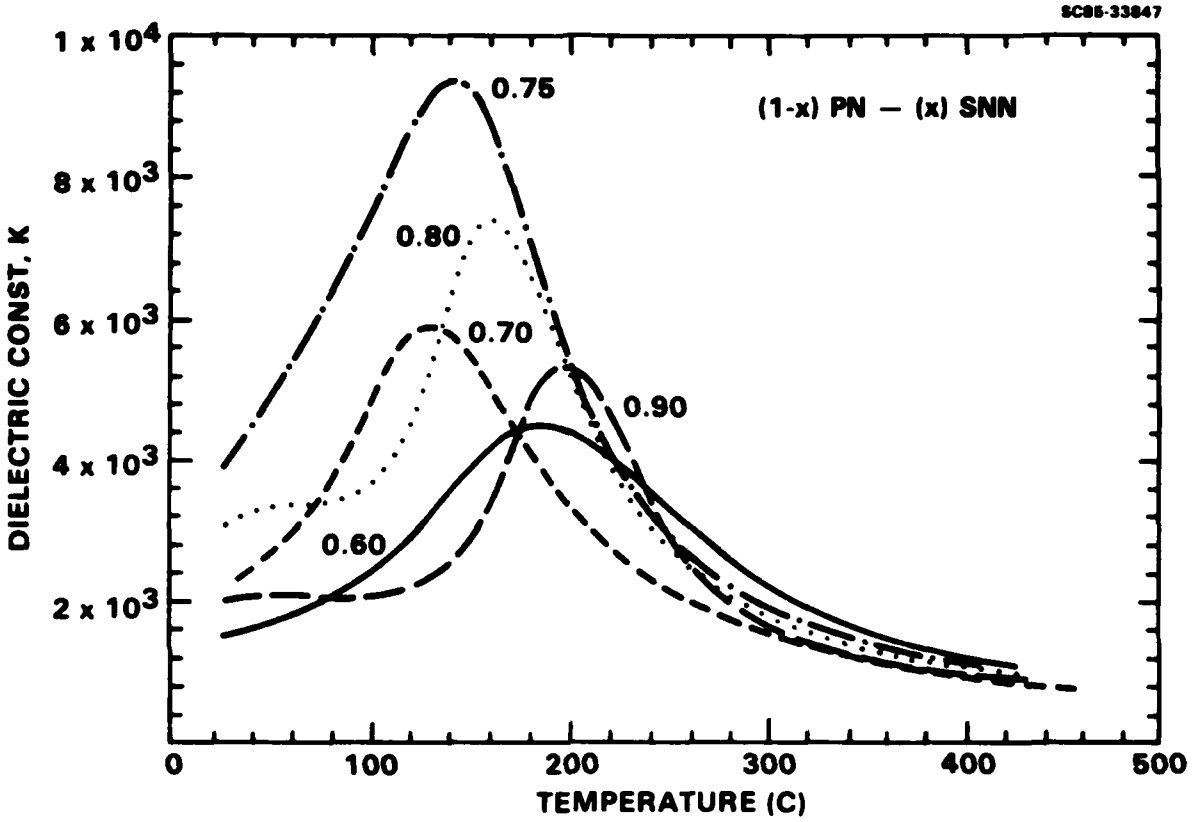

Fig. 17 Dielectric constant vs temperature for several PKN-SNN compositions. F = 10 kHz.

Both the PKN-SNN and PN-SNN systems look to be very promising candidates for optical crystal development. A major advantage in both systems, from a crystal growth standpoint, is that the more interesting compositions occur on the SNN-rich side of the phase diagrams, making homogeneous crystal growth a significantly easier task. Nevertheless, Pb^{2+} volatility at the melt temperatures is still a major concern, and more ceramic work is necessary to evaluate Pb^{2+} losses and dielectric and resistivity behavior as a function of time, temperature and initial PbO excess prior to Czochralski growth experiments.

6.0 FUTURE WORK

- Continue to improve the ADC Czochralski technique to develop optical quality crystals free of striations and other optical defects.

- Investigate suitable dopants, e.g., Ce^{3+}/Ce^{4+} and Fe^{2+}/Fe^{3+}, for enhancement of photorefractive sensitivity and speed using T.B. BSKNN-1 and BSKNN-2 crystals.

- Establish valence states and site preferences of the selected dopants in BSKNN-1 and BSKNN-2 crystals.

- Evaluation of optical quality and photorefractive properties, including sensitivity and speed, of the selected bronze crystals.

- Initiate the growth of compositions with potentially high electro-optic response, specifically compositions close to a morphotropic phase boundary in the PKN-SNN or PN-SNN systems.

7.0 REFERENCES

1. P.B. Jamieson, S.C. Abrahams and J.L. Bernstein, J. Chem. Phys. 50, 4352 (1969).

2. J. Ravez, A. Perron Simon and P. Hagenmuller, Ann. Chem. 12, 251 (1976).

3. M. DiDominico and S.H. Wemple, J. Appl. Phys. 40, 720 (1969).

4. R.R. Neurgaonkar and M.H. Kalisher, E.J. Staples and T.C. Lim, Appl. Phys. Lett. 35, 606 (1979).

5. R.R. Neurgaonkar, T.C. Lim, E.J. Staples and L.E. Cross, Ferroelectrics, 27, 62 (1980).

6. E.J. Staples, R.R. Neurgaonkar and T.C. Lim, Appl. Phys. Lett. 32, 197 (1978).

7. R.R. Neurgaonkar, Semi-Annual Report Nos. 3 and 4, Contract No. F49620-78-C-0093.

8. D. Berlincourt and H. Jaffe, Phys. Rev. 111, 143 (1958).

9. J.C. Toledano and J. Schneck, Solid State Comm. 16, 1101 (1975).

10. M.E. Lines and A.M. Glass, Principles and Applications of Ferroelectrics and Related Materials (Clarendon Press, Oxford) (1977).

11. B. Jaffe, W.R. Cook and H. Jaffe, Piezoelectric Ceramics (Academic Press, London and New York) (1971).

12. R.R. Neurgaonkar, Semi-Annual Technical Report No. 4, Contract No. N0014-82-C-2466.

13. L.E. Cross and R.R. Neurgaonkar, private communication.

14. J. Nakano and T. Yamada, J. Appl. Phys. 46, 2361 (1975).

15. K. Nagata, T. Yamazaki and K. Okazaki, Proc. 2nd Meeting on Ferroelectric Materials and Their Applications, 251 (1979).

END

DTIC

5-86